

## TECHNICAL NOTE

# Contrast-optimal simultaneous multi-slice bSSFP cine cardiac imaging at 0.55 T

Ye Tian<sup>1</sup> | Sophia X. Cui<sup>2</sup> | Yongwan Lim<sup>1</sup> | Nam G. Lee<sup>3</sup> | Ziwei Zhao<sup>1</sup> | Krishna S. Nayak<sup>1,3</sup>

<sup>1</sup>Ming Hsieh Department of Electrical and Computer Engineering, Viterbi School of Engineering, University of Southern California, Los Angeles, California, USA

<sup>2</sup>Siemens Medical Solutions USA, Los Angeles, California, USA

<sup>3</sup>Department of Biomedical Engineering, Viterbi School of Engineering, University of Southern California, Los Angeles, California, USA

## Correspondence

Ye Tian, Ming Hsieh Department of Electrical and Computer Engineering, Viterbi School of Engineering, University of Southern California, 3740 McClintock Ave, Los Angeles, CA EEB 428, USA.  
Email: [ytian607@usc.edu](mailto:ytian607@usc.edu)

## Funding information

American Heart Association, Grant/Award Number: 903839; National Heart, Lung, and Blood Institute, Grant/Award Number: R01-HL130494; National Science Foundation, Grant/Award Number: 1828736

**Purpose:** To determine if contemporary 0.55 T MRI supports the use of contrast-optimal flip angles (FA) for simultaneous multi-slice (SMS) balanced SSFP (bSSFP) cardiac function assessment, which is impractical at conventional field strengths because of excessive SAR and/or banding artifacts.

**Methods:** Blipped-CAIPI bSSFP was combined with spiral sampling for ventricular function assessment at 0.55 T. Cine movies with single band and SMS factors of 2 and 3 (SMS 2 and 3), and FA ranging from 60° to 160°, were acquired in seven healthy volunteers. Left ventricular blood and myocardial signal intensity (SI) normalized by background noise and blood–myocardium contrast were measured and compared across acquisition settings.

**Results:** Myocardial SI was slightly higher in single band than in SMS and decreased with an increasing FA. Blood SI increased as the FA increased for single band, and increment was small for  $FA \geq 120^\circ$ . Blood SI for SMS 2 and 3 increased with an increasing FA up to  $\sim 100^\circ$ . Blood–myocardium contrast increased with an increasing FA for single band, peaked at  $FA = 160^\circ$  (systole: 28.43, diastole: 29.15), attributed mainly to reduced myocardial SI when  $FA \geq 120^\circ$ . For SMS 2, contrast peaked at 120° (systole: 21.43, diastole: 19.85). For SMS 3, contrast peaked at 120° in systole (16.62) and 100° in diastole (19.04).

**Conclusions:** Contemporary 0.55 T MR scanners equipped with high-performance gradient systems allow the use of contrast-optimal FA for SMS accelerated bSSFP cine examinations without compromising image quality. The contrast-optimal FA was found to be 140° to 160° for single band and 100° to 120° for SMS 2 and 3.

## KEYWORDS

0.55 T, balanced steady-state free precession, blood–myocardium contrast, cardiac function, simultaneous multi-slice

This is an open access article under the terms of the [Creative Commons Attribution-NonCommercial License](https://creativecommons.org/licenses/by-nc/4.0/), which permits use, distribution and reproduction in any medium, provided the original work is properly cited and is not used for commercial purposes.

© 2022 The Authors. *Magnetic Resonance in Medicine* published by Wiley Periodicals LLC on behalf of International Society for Magnetic Resonance in Medicine.

## 1 | INTRODUCTION

MRI has steadily advanced toward higher field strengths and higher gradient performances, which has provided significant benefits for static high-resolution imaging of the brain, spine, and joints.<sup>1</sup> Meanwhile, cardiac MRI and other MRI applications of moving organs or the areas close to air-tissue boundaries are often preferentially performed using modern scanners with lowest available field strength, for example, 1.5 T.<sup>2</sup> There has been an increasing interest in exploring cardiac MRI on scanner configurations that operate at lower field strengths (<1 T) with high performance gradients.<sup>3–6</sup> This is because of the reduced susceptibility artifact, relaxed specific absorption rate (SAR) constraints, reduced off-resonance artifact, and beneficial scaling of physical parameters (shorter  $T_1$ , longer  $T_2$  and  $T_2^*$ ). A recent study by Bandettini et al.<sup>3</sup> has demonstrated that 0.55 T MRI can perform ventricular function assessment with diagnostic quality that is comparable to 1.5 T MRI. Another study by Restivo et al.<sup>4</sup> showed that high-performance 0.55 T MRI allows the use of highly SNR-efficient k-space trajectories. Moreover, MRI scanners operating at lower field strengths can potentially be manufactured at a lower cost, which, if passed onto the purchaser, can improve cardiac MRI access. Although 0.55 T cardiac MRI is promising, its full potential remains to be explored and its characteristics remain to be documented.

Cardiac cine MRI is routinely used to evaluate ventricular function, wall motion, and regional wall thickening. Balanced SSFP (bSSFP) is the preferred pulse sequence because it offers excellent SNR efficiency and blood–myocardium contrast. Standardized protocols<sup>7</sup> acquire a stack of short axis slices that cover the whole heart with multiple breath-holds (one per slice, 10–12 in total). Recently, simultaneous multi-slice (SMS) bSSFP techniques<sup>8–10</sup> have been used at 1.5 and 3 T to reduce the number of breath-holds by 2- to 4-fold. However, these studies used suboptimal flip angles (FA), mainly because of SAR constraints and banding artifacts, resulting in compromised image quality. For example, the study by Srinivasan and Ennis<sup>11</sup> reported a contrast-optimal FA of 105° for 1.5 T, and a recent 1.5 T SMS study used a FA of 54° and specified SAR as a limiting factor.<sup>9</sup> A higher FA can be used for 1.5 T SMS bSSFP while staying within SAR limits, however, this requires lengthening the RF pulse duration, which increases the TR, and generates unacceptable banding artifacts. Both the SAR constraint and  $B_0$  inhomogeneity are significantly relaxed at 0.55 T<sup>12</sup>; this provides new opportunities at 0.55 T to accelerate cardiac MRI examination without sacrificing image quality. Our hypothesis in this study is that contemporary 0.55 T

scanners<sup>12</sup> will allow the use of a contrast-optimal FA for SMS bSSFP.

For cardiac cine, it is important to note that blood is not in the steady state, and inflow blood contributes to the blood–myocardium contrast.<sup>11</sup> Previous in vivo studies suggested that the contrast-optimal FA is 130° at 0.35 T<sup>6</sup> and 105° at 1.5 T.<sup>11</sup> Three-dimensional bSSFP excites a thick slab and typically has reduced contrast compared to 2D bSSFP<sup>13</sup> mainly because the blood is closer to steady state. Although a static Bloch simulation suggested that FA of 68° provides optimal blood–myocardium contrast at 0.55 T,<sup>3</sup> to our knowledge, the contrast-optimal FA has not been documented at 0.55 T and effects of blood saturation have not been characterized for SMS bSSFP.

In this study, we implemented a blipped-CAIPI SMS bSSFP<sup>9</sup> combined with spiral sampling for ventricular function assessment at 0.55 T. In seven healthy volunteers, we acquired short-axis breath-hold cines for single band (also as SMS 1), SMS factors of 2 and 3 (or SMS 2 and SMS 3) with an FA range of 60° to 160° (20° increment). The systolic and diastolic signal intensities (SI) within left ventricular (LV) blood and LV myocardium were compared in the mid-ventricular slice. The difference in SI between mid-slice LV blood and myocardium (blood–myocardium contrast) was also compared across different SMS factors and FAs, and was used to determine the contrast-optimal FA.

## 2 | METHODS

### 2.1 | Pulse sequence

We implemented a blipped-CAIPI SMS bSSFP pulse sequence<sup>9</sup> combined with spiral readouts for cardiac cine, as shown in Figure 1. Slice encoding gradient blips were incorporated into the pre-winder and re-winder of the slice-selective gradients (Figure 1B,C) to minimize the TR. These blips encode the simultaneously acquired slices such that these slices have a phase modulation of  $\Phi_{ab} = e^{2\pi i(a-1)(b-1)/N_{\text{SMS}}}$  for the  $a$  th slice and  $b$  th slice encoding gradient. A single-slice RF excitation pulse was designed with the Shinnar-Le Roux algorithm<sup>14</sup> and then superimposed with frequency-modulated versions to form an SMS RF pulse. We used optimized phase schedules<sup>15</sup> to reduce the peak  $B_1$ . Note that the limiting factor for the SMS pulse design at 0.55 T is not SAR, but the peak  $B_1$ . For each subject, the scanner performs a pre-scan calibration to determine the maximum allowed  $B_1$ . To ensure that our results are generalizable to variation in the loading (e.g., variation in patient weight), we used a conservative peak  $B_1$  value of 19  $\mu\text{T}$  in all our pulse designs. The readout was a  $M_1$ -nulled uniform density spiral trajectory (Figure 1D),

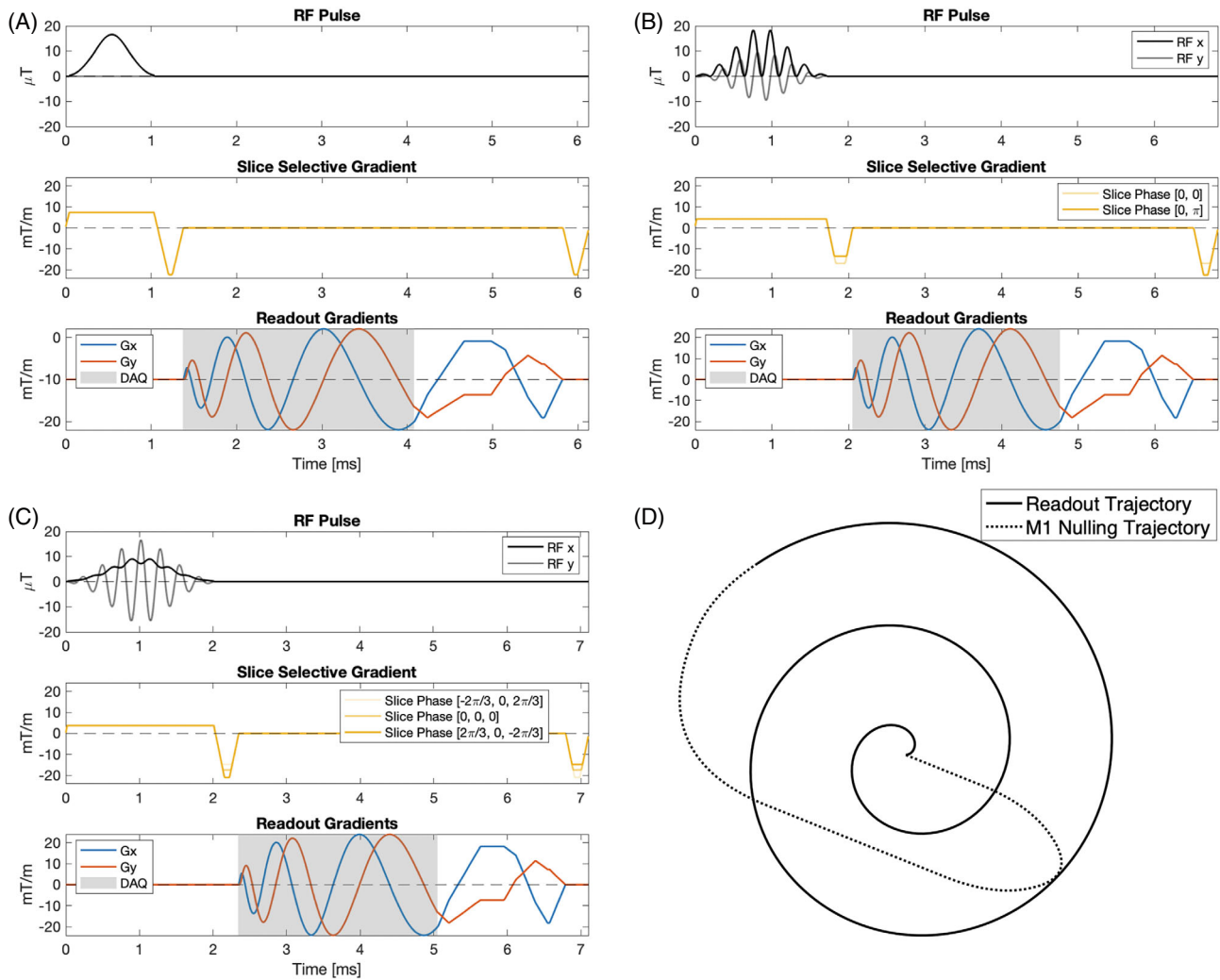


**FIGURE 1** Pulse sequence diagrams. Pulse sequences for (A) single band, (B) SMS 2 and (C) SMS 3 with  $FA = 120^\circ$  are shown. The RF phase for each slice is optimized to minimize peak  $B_1$ . For SMS 2 and SMS 3, RF peak value is 1.89 and 2.17 times of single-slice RF, respectively. RF duration is minimized under the peak  $B_1$  limitation ( $19 \mu T$ ). Blipped-CAIPI phase modulation gradients are incorporated into the pre-winder and re-winder of the slice-selective gradient to reduce the TR. A (D)  $M_1$ -nulled spiral-out trajectory is used, where the DAQ duration is 2.71 ms and the moment nulling duration is 1.74 ms. SMS, simultaneous multi-slice; FA, flip angle; DAQ, data acquisition

with a readout duration of 2.7 ms and a FOV of 50 cm with 72 interleaves.

The trajectory order for electrocardiogram-triggered cine is illustrated in Figure 2. The sequence acquires data from 12 heartbeats for SMS 1 and 2, and acquires data from 15 heartbeats for SMS 3, resulting in acceleration factors of 1, 2, and 2.4 fold for SMS 1, 2, and 3, respectively. A segmented acquisition strategy was used, where the entire k-space was divided into number of heartbeats ( $N_{hb}$ ) segments, and each heartbeat acquires one segment of k-space. Six spirals from each heartbeat are combined to reconstruct one cardiac phase. There are 360 unique spirals in the entire trajectory. Each group of six spirals have an initial spiral angle at  $k \times 60/N_{hb} + l \times 360/N_{hb} + \theta_m$ , where  $k = 0, 1, \dots, 5$  is the spiral index,  $l = 0, 1, \dots, N_{hb} - 1$  is the heartbeat index, and  $\theta_m$  ( $m = 0, 1, \dots, 60/N_{hb}$ ) is

an offset angle, which can distribute the sampling such that adjacent groups have a maximum sampling angle difference (e.g.,  $\theta_m = [0, 2, 4, 1, 3]$  for  $N_{hb} = 12$  and  $\theta_m = [0, 2, 1, 3]$  for  $N_{hb} = 15$ ). This will ensure data inconsistency in the spatial and temporal domains to favor for the constrained reconstruction.<sup>16</sup> For SMS sampling, slice encoding gradient (or SMS phase modulation) order has a shift between the  $360/N_{hb}$  spirals, as illustrated in Figure 2 for SMS 2.

## 2.2 | Acquisition

Seven healthy volunteers (4 male/3 female, age,  $28 \pm 4$ , heart rate,  $62 \pm 6$  bpm) were recruited for this study. Our institutional review board approved the study and

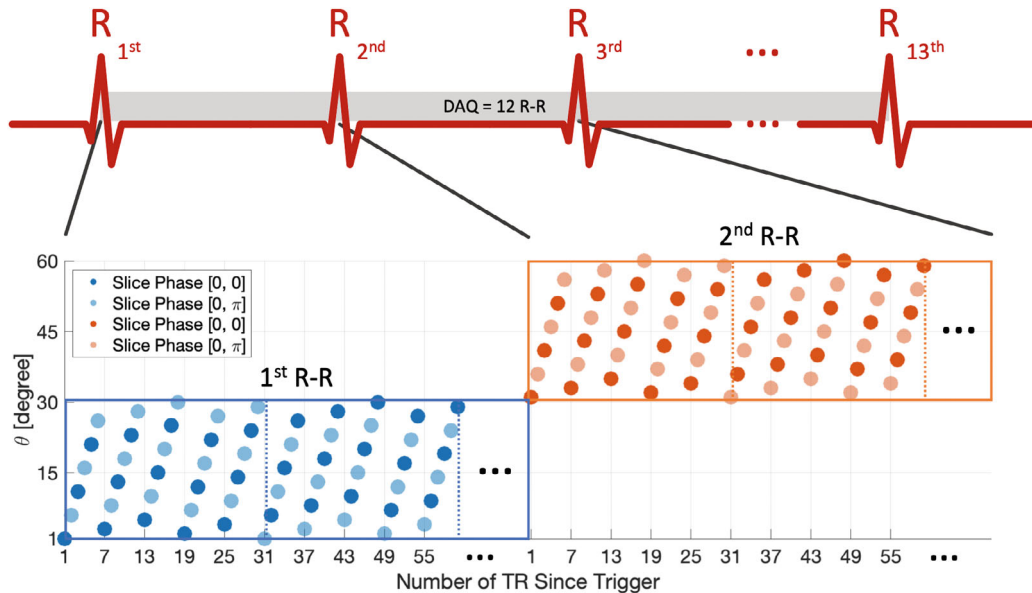


**FIGURE 2** Sampling scheme for SMS 2 bSSFP cine. Data acquisition duration is 12 heartbeats ( $N_{hb}$ ) for single band and SMS 2, and 15 heartbeats for SMS 3 (not shown). Each heartbeat acquires one segment of k-space, and the entire k-space is divided into  $N_{hb}$  segments. Within each heartbeat, each group of six arms is equally spaced, and a rotation is added between groups that maximizes the sampling angle difference between adjacent groups. The sampling order of  $360/N_{hb}$  spiral arms will be repeated until a trigger is received and each group of  $360/N_{hb}$  spirals has a slice encoding shift (color coded). SMS, simultaneous multi-slice; bSSFP, balanced SSFP;  $N_{hb}$ , number of heartbeats

written informed consent was obtained from all volunteers. Experiments were performed using a whole-body 0.55 T system (prototype MAGNETOM Aera, Siemens Healthcare) equipped with high-performance shielded gradients (45 mT/m amplitude, 200 T/m/s slew rate). Imaging was performed using the RTHawk system (HeartVista).<sup>17</sup> The integrated body coil was used for RF transmission. A six-element surface body coil (anterior) and six elements from an 18-element spine array (posterior) were used for signal reception. Other scan parameters were spatial resolution =  $1.5 \times 1.5 \text{ mm}^2$ , slice thickness = 8 mm, RF time bandwidth product = 1.5, TR and TE varied from 5.8–7.1 ms and 0.9–1.4 ms, respectively, because of RF duration differences. FA ranging from  $60^\circ$  to  $140^\circ$  ( $20^\circ$  increment) was acquired for all SMS factors. Additionally, FA of  $160^\circ$  cines were acquired with single band. A short-axis slice in the middle of the LV myocardium (referred to as the mid slice) was prescribed for single band. SMS cines acquired one slice at the mid slice position and simultaneously acquired one more slice at 2.4 cm toward the basal direction (SMS 2) or two more slices at 2.4 cm toward both the basal and apical directions (SMS 3). For SMS 2, additional cines with FA of  $120^\circ$  were acquired at mid and apical slices in three volunteers. A voice command was given to perform end-exhale breath hold for each data acquisition, lasting for 10 to 17 s each because of heart rate and sequence differences.

### 2.3 | Reconstruction

Image reconstruction used gradient impulse response functions (GIRF)<sup>18</sup> corrected spiral trajectory. All images were reconstructed using spatiotemporal constrained reconstruction<sup>16</sup> with necessary modification for SMS.<sup>19</sup> Specifically, the following cost function was solved with a conjugate gradient algorithm with a line search:

$$\|Am - d\|_2^2 + \lambda_s \left\| \sqrt{(\nabla_x m)^2 + (\nabla_y m)^2 + \epsilon} \right\|_1 + \lambda_t \left\| \sqrt{(\nabla_t m)^2 + \epsilon} \right\|_1,$$

where  $d$  is multi-coil k-space data,  $A = \Phi FS$  is the encoding matrix that includes phase modulation  $\Phi$  for CAIPI, non-uniform Fourier transform  $F$  and coil sensitivities  $S$  estimated by the Walsh method,<sup>20</sup>  $m$  represents images to be reconstructed,  $\lambda_{t,s}$  are temporal and spatial regularization parameters, and  $\epsilon$  is a small positive value used to avoid singularity issues. The regularization parameters ( $\lambda_t = 2e^{-3}S$  and  $\lambda_s = 5e^{-4}S$ , where  $S$  is the highest pixel intensity in  $A^{-1}d$ ) were chosen from a parameter sweep, and by using both L-curve and qualitative assessments. Details of the parameter selection are provided in the Supporting Information Reconstruction Parameter Selection, with Figure S1 and Video S1 representing reconstruction results with different parameters.

k-Space data was sorted to have six spirals from each heartbeat for each cardiac phase, resulting in a temporal resolution of  $\sim 40$  ms/cardiac phase. The number of cardiac phases during reconstruction was determined from the median duration of all heartbeats. For heartbeats longer than the median duration, the data acquired at the end of the cardiac cycle was discarded. For heartbeats shorter than the median duration, the unacquired k-space data was borrowed from the closest cardiac phase. This is usually not problematic because both the borrowing phase and the borrowed phase are at the quiescent end-diastolic phase where there is little motion. The first nine spiral arms were discarded because steady state was not established at the beginning of each acquisition. After reconstruction, cine movies were interpolated to 25 cardiac phases.

All images were reconstructed offline in MATLAB 2021a (The MathWorks) and on a server equipped with 4× AMD EPYC 7502 32-Core CPU, 504Gb CPU memory, 4× NVIDIA A100 GPU, and 40Gb GPU memory for each core. The iterative part of the algorithm was performed on a single GPU core and the other reconstruction was performed on the CPU.

## 2.4 | Analysis

One systolic and one diastolic phase were selected in the mid slice of each acquisition to calculate blood and myocardial SI and blood–myocardium contrast. The mid-slice images across different SMS factors and FAs were first registered by a translation-only registration to compensate for breath holding mismatches. Registered images were averaged across different SMS factors and FAs. Manual regions of interest (ROIs) for LV blood and myocardium were drawn conservatively on the averaged image and were applied to each image individually. The SIs were normalized by noise measurements that were obtained from each volunteer. Because the constrained reconstruction can change the noise distribution, we measured the noise from gridding reconstruction of single-band cine acquired with FA of  $120^\circ$ , by using a set of fully sampled data (72 spiral arms) from the end-diastolic phase. An ROI was drawn in the background where no artifacts are seen, and the SD within the ROI was calculated as the noise level. Averaged SI within LV blood and LV myocardium ROIs were reported, and their difference was reported as blood–myocardium contrast.

## 3 | RESULTS

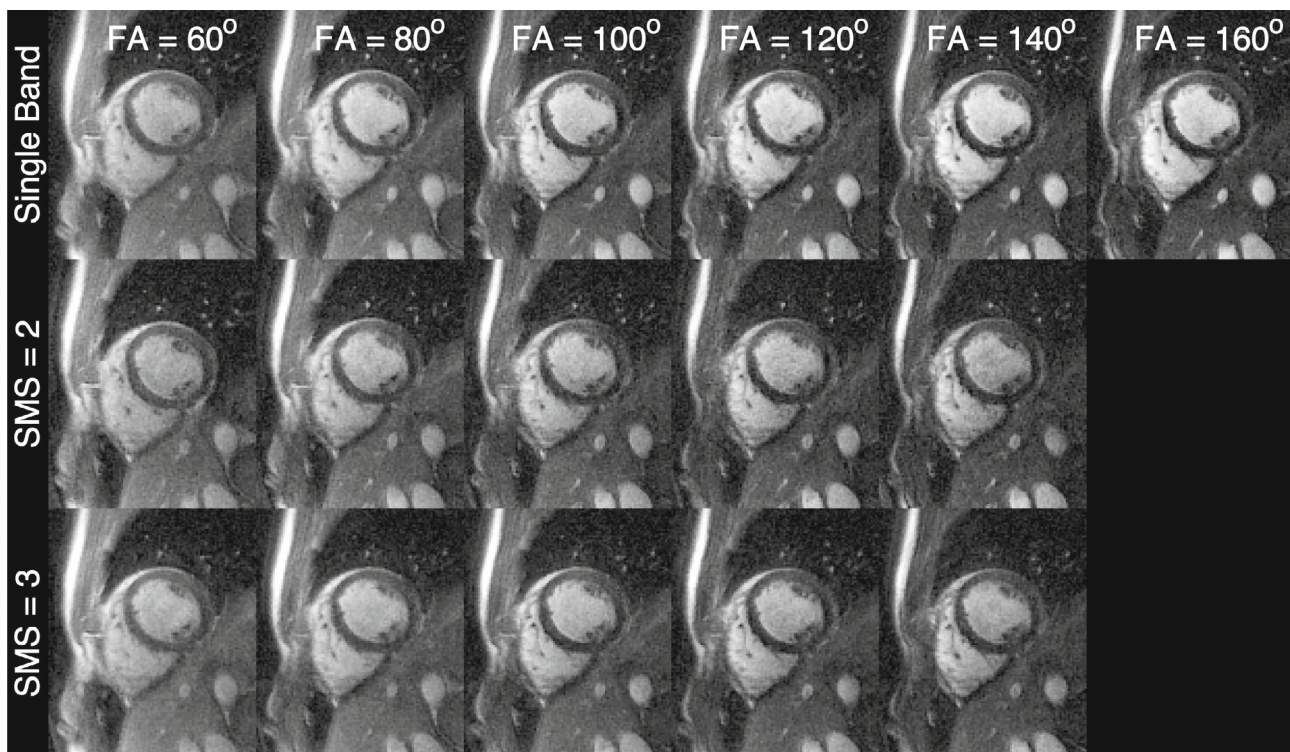
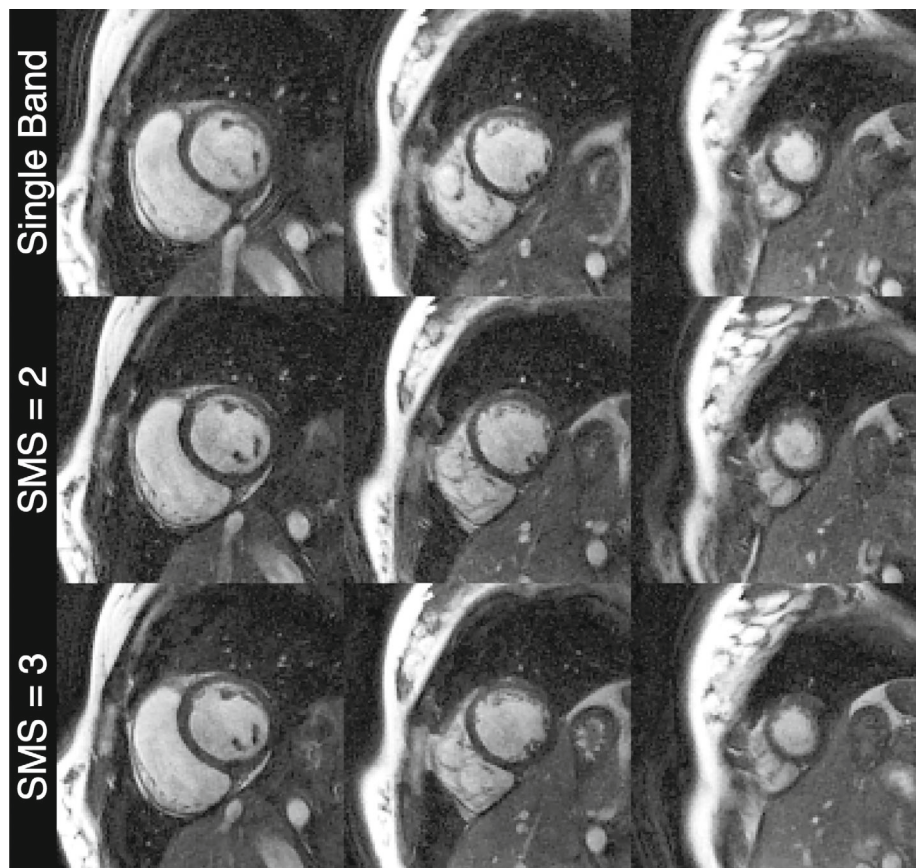
The combination of slice gradient blips into the slice encoding gradients reduced the TR by 0.3 ms. The use

of optimized phase RF combination resulted in the peak  $B_1$  being 1.89 and 2.17 times that of the single band RF for SMS 2 and 3, respectively. This allowed reduction of the RF duration by 5.5% for SMS 2 and 24% for SMS 3, corresponding to 0.1 ms and 0.8 ms at FA =  $120^\circ$  for SMS 2 and 3, respectively. The average per-slice reconstruction time across all subjects was  $83.28 \pm 21.00$  s,  $67.57 \pm 11.20$  s, and  $69.04 \pm 15.04$  s for SMS 1, 2, and 3, respectively.

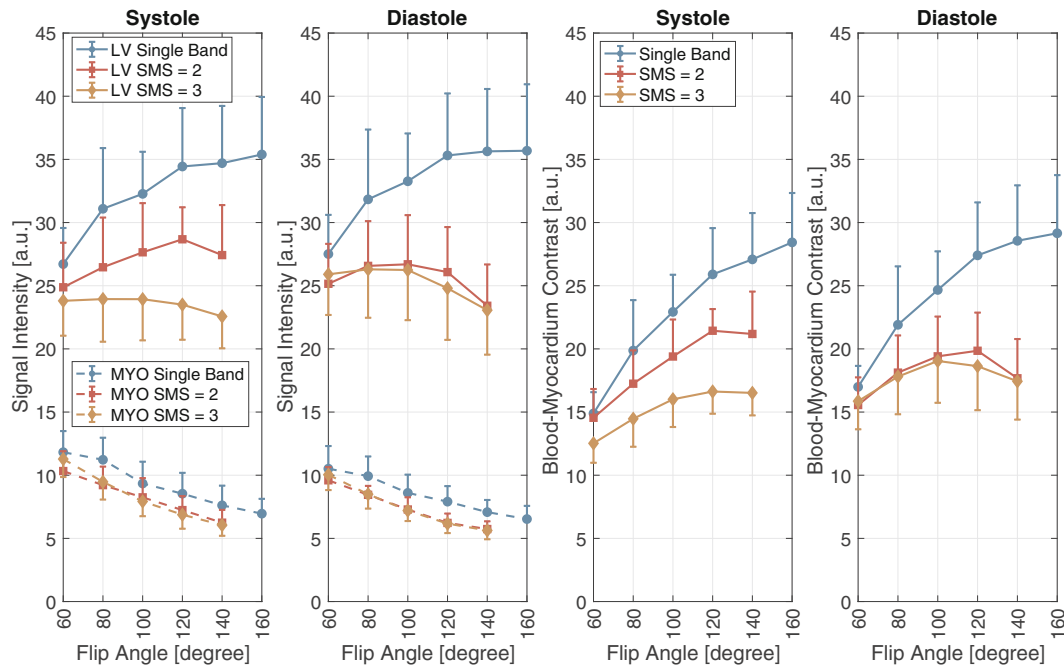
Figure 3 compares the image quality between single band and SMS cines at FA =  $120^\circ$ . For qualitative assessment, we focused on the clarity of endocardial and epicardial boundaries throughout the cardiac cycle, because these are critical in evaluating LV function, including LV ejection fraction and regional LV wall thickening. No visual image quality difference was detected for the different SMS factors. We did not observe banding artifact across all SMS factors (TR durations were different) in the cardiac ROIs. Video S2 shows the corresponding cine videos, from which we can observe that flow artifacts appear slightly different, however the LV boundaries are clearly depicted. Flow artifact differences were likely caused by the differences in slice encoding gradients and RF durations. Video S3 shows mid-slice cine videos obtained from all subjects with SMS 1, 2, and 3, where we obtained consistent high-quality cines for all subjects.

Figure 4 compares the mid-slice cine images acquired with different FAs and SMS factors for one volunteer and Video S4 shows the corresponding video. Figure 5 shows the quantitative signal intensities and blood–myocardium contrast averaged across seven volunteers. Within the tested FA range ( $60^\circ$ – $160^\circ$  for single band and  $60^\circ$ – $140^\circ$  for SMS 2 and 3), myocardial SI decreases with a higher FA for all SMS factors, and the single band myocardial SI is higher than SMS 2 and 3. Blood SI increases with a high FA for single band, peak SI observed was 35.39 for systole and 35.68 for diastole at FA =  $160^\circ$ , but the increment is minimal for FA  $\geq 120^\circ$  (from  $120^\circ$ – $160^\circ$ , the SI increment was 3% and 1% for systole and diastole, respectively). For SMS 2, blood SI increases with increasing FA and peaked at FA =  $120^\circ$  for systole (28.68) and at  $100^\circ$  for diastole (26.70). For SMS 3, blood SI increases with increasing FA and peaked at FA =  $80^\circ$  for both systole (23.94) and diastole (26.30). Blood–myocardium contrast for single band was higher as FA increases and is largely because of reduced myocardial SI when FA  $\geq 120^\circ$ . The peak contrast for single band was 28.43 for systole and 29.15 for diastole at FA =  $160^\circ$ . For SMS 2, blood–myocardium contrast reached peak at  $120^\circ$  (systole: 21.43, diastole: 19.85), and for SMS 3 contrast was peak at  $120^\circ$  in systole (16.62) and at  $100^\circ$  in diastole (19.04). SMS generally provided lower blood signals and lower contrasts.

**FIGURE 3** Representative comparison of mid short-axis cine acquired at different SMS factors and  $FA = 120^\circ$ . Images between single band and SMS 2 and 3 have no visual image quality difference and slightly different flow effects (can be seen in Video S2). This is because the images were acquired with different RF durations and slice encoding gradients. LV-myocardium contrast is slightly different as expected, with the SMS excitation saturating the outer volume of blood, which decreases the inflowing blood signal intensity. SMS, simultaneous multi-slice; FA, flip angle; LV, left ventricular



**FIGURE 4** Representative comparison of mid short-axis cine acquired with different SMS factors and FAs. Figure shows a mid short-axis slice end-diastole cine image for single band, SMS 2 and 3 acquired at different FAs. For single band image, the apparent contrast is higher with a higher FA. For SMS, the contrast increase with FA is present but reduced compared to single band. The overall image contrast is slightly less in SMS than in single band. Corresponding video can be found in the Video S4. As FA goes up, the RF duration has to be elongated to reduce the peak  $B_1$ , which increases the flow artifacts. SMS, simultaneous multi-slice; FA, flip angle



**FIGURE 5** Blood–myocardium contrasts and signal intensities. Figure shows the averaged blood–myocardium contrast during end-systole and end-diastole (left two plots) and averaged blood and myocardial signal intensities during end-systole and end-diastole (right two plots). For single band acquisition, the contrast increases with the FA and is largely because of the suppressed myocardial signal. The incremental improvement in blood SI is small for  $FA \geq 120^\circ$ . For SMS acquisitions, the blood-tissue contrast starts to decrease when  $FA \geq 100\text{--}120^\circ$ , largely because of the reduced blood signal. FA, flip angle; SI, signal intensity

## 4 | DISCUSSION

In this study, we demonstrate that contemporary 0.55 T MRI with high-performance gradients allows for contrast-optimal FA being used for SMS bSSFP cine, which is impractical at higher field strengths. We specifically demonstrated a blipped-CAIPI SMS bSSFP spiral pulse sequence for cardiac function assessment at 0.55 T. The SMS image quality was comparable to that of the single band and has lower blood–myocardium contrast at the same FA, likely because of inflowing blood being partially saturated by SMS excitation and blipped-CAIPI SMS phase modulation.

In the SMS pulse sequence design, we used Shinnar-Le Roux to design single-band RF and superimposed frequency-modulated versions by the optimized phase combination.<sup>15</sup> This design may not always generate the minimal RF duration and peak  $B_1$  compared with more advanced RF designs such as using optimal control.<sup>21</sup> However, the scan plane for the heart is always double-oblique, the use of varying slice encoding gradients, which is common in optimal control designed gradients, may suffer from gradient imperfections<sup>21</sup> and concomitant fields.<sup>22</sup> Note that these imperfections in encoding can be corrected with post-corrections such as done in this study by using GIRF-predicted

trajectories<sup>18</sup> or more advanced high order reconstruction<sup>23</sup>; the slice selective gradient may need to be corrected with pre-compensation,<sup>21,24</sup> which requires calculation on-the-fly for double-oblique scans.

We have acquired cardiac cine with FAs from  $60^\circ$  to  $160^\circ$  for single band and from  $60^\circ$  to  $140^\circ$  for SMS. For SMS, we have reached peak contrast as shown in Figure 5, however, the peak contrast was not reached for the single band in the tested FA range. For single band, we noticed that the SI in the blood plateaued after  $FA \geq 120^\circ$ , and the increased blood–myocardium contrast is mainly from the decreased myocardial SI. The contrast increased as FA goes higher, however, overall image quality did not, as can be seen from Figure 4 and Video S3. One potential reason is that when FA increases under a maximum allowed  $B_1$ , the RF duration needs to be increased (and so is TR), which will lead to more sensitivity to banding and inflow artifacts. For these practical reasons, we did not investigate  $FA > 160^\circ$  for single band. Another limitation of the study is that we only quantitatively demonstrated the optimal FA for different SMS factors, but the images were not evaluated by experienced readers, so the optimal FA for diagnostic purpose was not determined.

We used a spiral-out trajectory in this study instead of the more commonly used Cartesian sampling. To the best of our knowledge, this study is the first to

document the combination of SMS bSSFP and spiral readouts. Non-Cartesian SMS has some advantages, notably the improved sampling SNR efficiency and the fact that the aliasing pattern appears noise-like when combined with CAIPI phase modulation.<sup>25</sup> Non-Cartesian SMS techniques have been applied mainly in cardiac MRI to reduce the scan time or acquire more slices in a limited time, such as first-pass myocardial perfusion.<sup>19,26–29</sup> The incoherent aliasing pattern of non-Cartesian trajectories also benefits constrained reconstruction. Our study did not use a high undersampling rate, but there is potential for greater acceleration with more aggressive regularization, as shown in Figure S2 where the reconstruction was performed on SMS 3 with an undersampling rate of 7.2. Moreover, spiral trajectories and their variants are flexible in readout duration, and the scan efficiency (duty cycle) increases with the readout time. The spiral-out trajectory used in this study had a duty cycle of 38% to 44%, and a spiral in-out trajectory may achieve a duty cycle of 69%<sup>4</sup> or higher, but may suffer more from flow artifacts because  $M_1$  is not nulled at the echo time. Further study may optimize the trajectory for a higher undersample rate.

This study used a whole-body 0.55 T scanner with a high-performance gradient system capable of 45 mT/m amplitude and 200 T/m/s slew rate. This is a “ramped down” version of a commercially available 1.5 T system, first described by Campbell-Washburn et al.<sup>12</sup> At this time, there is a commercially available whole-body 0.55 T system (MAGNETOM Free.Max, Siemens Healthcare) that has gradients capable of 15 mT/m amplitude and 40 T/m/s slew rate. In the sequence design we did not use the maximum gradient specification, instead we used 24 mT/m gradient amplitude and 180 T/m/s slew rate. Spiral trajectory design is limited by the gradient performance. For example, if a lower slew rate of 40 T/m/s was used, to keep the same undersampling rate each spiral readout will be prolonged by 5.6 ms (so is TR), which may not be acceptable because of the increased flow artifacts and banding artifacts.

We note that the SI of blood and myocardial are lower in SMS acquisitions than in single band acquisitions. The reasons are 2-fold. First, the blipped-CAIPI phase modulation introduces a phase across the excited imaging slice, resulted in a signal loss as a function of slice thickness and SMS slice gap.<sup>30</sup> This and the difference in TE contribute most of the signal difference in the myocardium. Second, in the blood, saturation because of SMS excitation can decrease the signal level. For cardiac cine, a large portion of the signal is contributed by the inflow that has equilibrium magnetization.<sup>11</sup> SMS pulses excite larger blood volume, decreasing the inflow blood signal. We show the mid-slice LV blood signals of single band and SMS 2 and 3 in Figure S3. Two different scenarios for SMS

2 are shown: SMS 2 with simultaneously acquiring mid and base slices (SMS 2, M/B) and SMS 2 acquiring mid and apex slices (SMS 2, M/A). Omit the complex turbulence blood flow, during systole most blood moves from apex toward base, during diastole the blood moves from base to apex. The single band SI curve has the highest value among all curves and shows two peaks that correspond to the inflow blood in systole and diastole. For SMS 2, M/A, blood flowing from apex to mid during systole is saturated by excitation in the apex slice, resulting in a lower SI in the mid slice for SMS 2, M/A than SMS 2, M/B. During diastole, the bulk blood flow direction is changed, resulting in blood SI in the mid slice being lower in SMS 2, M/B than that in SMS 2, M/A. Images acquired with SMS 3 has the lowest SI among all curves because of the largest excitation volume. The contrast-optimal FA at 0.55 T (FA = 140°–160° for single band, FA = 100°–120° for SMS 2 or 3) found in this study also differed from 68°, which was determined by Bloch simulation that does not include flow effects.<sup>3</sup>

## 5 | CONCLUSION

We demonstrate that cardiac function imaging at 0.55 T can be expedited using SMS techniques (factor of 2 or 3) without any significant compromise in image quality. Furthermore, it is possible to use contrast-optimal FA at 0.55 T, specifically 140° to 160° for single band and 100° to 120° for SMS factors of 2 or 3.

## ACKNOWLEDGMENT

We acknowledge research support from Siemens Healthineers.

## FUNDING INFORMATION

National Science Foundation, Grant/Award Number: 1828736; National Institutes of Health, Grant/Award Number: R01-HL130494; American Heart Association, Grant/Award Number: 903839

## CONFLICT OF INTEREST


Sophia X. Cui is an employee of Siemens Healthineers.

## DATA AVAILABILITY STATEMENT


One representative SMS dataset with reconstruction code is available at: [https://github.com/usc-mrel/lowfield\\_spiral\\_sms\\_cine](https://github.com/usc-mrel/lowfield_spiral_sms_cine). The rest datasets used and/or analyzed during the current study are available from the corresponding author on reasonable request.

## ORCID


Ye Tian  <https://orcid.org/0000-0002-8559-4404>

Yongwan Lim  <https://orcid.org/0000-0003-0070-0034>



Nam G. Lee  <https://orcid.org/0000-0001-5462-1492>

Ziwei Zhao  <https://orcid.org/0000-0003-0281-1141>

Krishna S. Nayak  <https://orcid.org/0000-0001-5735-3550>

## REFERENCES

- Ladd ME, Bachert P, Meyerspeer M, et al. Pros and cons of ultra-high-field MRI/MRS for human application. *Prog Nucl Magn Reson Spectrosc.* 2018;109:1-50.
- Nayak KS, Lim Y, Campbell-Washburn AE, Steeden J. Real-time magnetic resonance imaging. *Journal of Magnetic Resonance Imaging.* 2022;55:81-99.
- Bandettini WP, Shanbhag SM, Mancini C, et al. A comparison of cine CMR imaging at 0.55 T and 1.5 T. *J Cardiovasc Magn Reson.* 2020;22:37.
- Restivo MC, Ramasawmy R, Bandettini WP, Herzka DA, Campbell-Washburn AE. Efficient spiral in-out and EPI balanced steady-state free precession cine imaging using a high-performance 0.55T MRI. *Magn Reson Med.* 2020;84:2364-2375.
- Varghese J, Craft J, Crabtree CD, et al. Assessment of cardiac function, blood flow and myocardial tissue relaxation parameters at 0.35 T. *NMR Biomed.* 2020;33:e4317.
- Rashid S, Han F, Gao Y, et al. Cardiac balanced steady-state free precession MRI at 0.35 T: a comparison study with 1.5 T. *Quant Imaging Med Surg.* 2018;8:627-636.
- Kramer CM, Barkhausen J, Bucciarelli-Ducci C, Flamm SD, Kim RJ, Nagel E. Standardized cardiovascular magnetic resonance imaging (CMR) protocols: 2020 update. *J Cardiovasc Magn Reson.* 2020;22:17.
- Nazir MS, Neji R, Speier P, et al. Simultaneous multi slice (SMS) balanced steady state free precession first-pass myocardial perfusion cardiovascular magnetic resonance with iterative reconstruction at 1.5 T. *J Cardiovasc Magn Reson.* 2018;20:84.
- Price AN, Cordero-Grande L, Malik SJ, Hajnal JV. Simultaneous multislice imaging of the heart using multiband balanced SSFP with blipped-CAIPI. *Magn Reson Med.* 2020;83:2185-2196.
- Stüb D, Speier P. Gradient-controlled local Larmor adjustment (GC-LOLA) for simultaneous multislice bSSFP imaging with improved banding behavior. *Magn Reson Med.* 2019;81:129-139.
- Srinivasan S, Ennis DB. Optimal flip angle for high contrast balanced SSFP cardiac cine imaging. *Magn Reson Med.* 2015;73:1095-1103.
- Campbell-Washburn AE, Ramasawmy R, Restivo MC, et al. Opportunities in interventional and diagnostic imaging by using high-performance low-field-strength MRI. *Radiology.* 2019;293:384-393.
- Mascarenhas NB, Muthupillai R, Cheong B, Pereyra M, Flamm SD. Fast 3D cine steady-state free precession imaging with sensitivity encoding for assessment of left ventricular function in a single breath-hold. *AJR Am J Roentgenol.* 2006;187:1235-1239.
- Pauly J, Le Roux P, Nishimura D, Macovski A. Parameter relations for the Shinnar-Le Roux selective excitation pulse design algorithm [NMR imaging]. *IEEE Trans Med Imaging.* 1991;10:53-65.
- Wong E. Optimized Phase Schedules for Minimizing Peak RF Power in Simultaneous Multi-Slice RF Excitation Pulses. ISMRM 20th annual meeting; 2012; Melbourne, Australia.
- Adluru G, McGann C, Speier P, Kholmovski EG, Shaaban A, Dibella EV. Acquisition and reconstruction of undersampled radial data for myocardial perfusion magnetic resonance imaging. *J Magn Reson Imaging.* 2009;29:466-473.
- Santos JM, Wright GA, Pauly JM. Flexible real-time magnetic resonance imaging framework. *Conf Proc IEEE Eng Med Biol Soc.* 2004;2004:1048-1051.
- Campbell-Washburn AE, Xue H, Lederman RJ, Faranesh AZ, Hansen MS. Real-time distortion correction of spiral and echo planar images using the gradient system impulse response function. *Magn Reson Med.* 2016;75:2278-2285.
- Tian Y, Mendes J, Pedgaonkar A, et al. Feasibility of multiple-view myocardial perfusion MRI using radial simultaneous multi-slice acquisitions. *PLoS One.* 2019;14:e0211738.
- Walsh DO, Gmitro AF, Marcellin MW. Adaptive reconstruction of phased array MR imagery. *Magn Reson Med.* 2000;43:682-690.
- Aigner CS, Rund A, Abo Seada S, et al. Time optimal control-based RF pulse design under gradient imperfections. *Magn Reson Med.* 2020;83:561-574.
- King KF, Ganin A, Zhou XJ, Bernstein MA. Concomitant gradient field effects in spiral scans. *Magn Reson Med.* 1999;41:103-112.
- Lee NG, Ramasawmy R, Lim Y, Campbell-Washburn AE, Nayak KS. MaxGIRF: image reconstruction incorporating concomitant field and gradient impulse response function effects. *Magn Reson Med.* 2022;88:691-710.
- Zhao Z, Lee NG, Nayak KS. Multidimensional RF Pulse Design with Known Spatial Encoding Imperfections. ISMRM 2021; 3954.
- Yutzy SR, Seiberlich N, Duerk JL, Griswold MA. Improvements in multislice parallel imaging using radial CAIPIRINHA. *Magn Reson Med.* 2011;65:1630-1637.
- Tian Y, Mendes J, Wilson B, et al. Whole-heart, ungated, free-breathing, cardiac-phase-resolved myocardial perfusion MRI by using continuous radial interleaved simultaneous multi-slice acquisitions at sSpoiled steady-state (CRIMP). *Magn Reson Med.* 2020;84:3071-3087.
- Wang J, Yang Y, Weller DS, et al. High spatial resolution spiral first-pass myocardial perfusion imaging with whole-heart coverage at 3 T. *Magn Reson Med.* 2021;86:648-662.
- Yang Y, Meyer CH, Epstein FH, Kramer CM, Salerno M. Whole-heart spiral simultaneous multi-slice first-pass myocardial perfusion imaging. *Magn Reson Med.* 2019;81:852-862.
- Wang H, Adluru G, Chen L, Kholmovski EG, Bangerter NK, DiBella EV. Radial simultaneous multi-slice CAIPI for ungated myocardial perfusion. *Magn Reson Imaging.* 2016;34:1329-1336.
- Setsompop K, Gagoski BA, Polimeni JR, Witzel T, Wedeen VJ, Wald LL. Blipped-controlled aliasing in parallel imaging for simultaneous multislice echo planar imaging with reduced g-factor penalty. *Magn Reson Med.* 2012;67:1210-1224.

## SUPPORTING INFORMATION

Additional supporting information may be found in the online version of the article at the publisher's website.

**FIGURE S1.** (A) 3D plot of the parameter sweeping results (B) selected reconstructions with different regularization parameters. This figure shows parameter sweep results from one SMS 3 dataset acquired with  $FA = 120^\circ$ . Ideally, the 3D plot of norms can show an obvious  $L$  shape on both the temporal-fidelity and the spatial-fidelity planes, and the parameters selected would be at the corner of the  $L$  shape. The results are condensed along the temporal-spatial diagonal as shown in (A) because the TV and the TFD norms are correlated. Additionally,  $L$  shape of the temporal-fidelity is less apparent than that of the spatial-fidelity because of the high temporal redundancy in the cine data. We show images reconstructed with different regularization parameters in (B) with the selected reconstruction marked by a red box and the corresponding videos are shown in Video S1. For each image, the left shows a diastolic phase, and two intensity versus time line-plots are shown in the middle (blue line) and the right (orange line). The regularization parameters were chosen qualitatively based on a desirable trade-off between the temporal blurring and the apparent noise level. More details of the parameter sweep and the selection of parameters can be found in the Supporting Information.

**FIGURE S2.** Retrospectively undersampled reconstruction for SMS 3. (Top) SMS 3 (undersample rate of 2.4) with the sampling and reconstruction methods described in the paper and (bottom) retrospective  $3\times$  undersampling (undersample rate of 7.2) reconstructed with STCR. The retrospective  $3\times$  undersampling can potentially allow for nine slices of cine being acquired within 15 heartbeats, which is within one breath hold for most patients. With more aggressive regularization parameters ( $\lambda_t = 5e^{-3}$ ,  $\lambda_s = 1e^{-3}$ , compared with  $\lambda_t = 2e^{-3}$ ,  $\lambda_s = 5e^{-4}$  for the original sampling), the retrospective  $3\times$  undersampled reconstruction can achieve a similar image quality as the original sampling.

**FIGURE S3.** Representative mid-slice LV blood signal intensity curves in one cardiac cycle. The left image shows the slice positions on a 4-chamber view. The signal intensity curves of mid-slice LV blood for single band, SMS 2 and 3 are displayed on the right. The SI curve of single band has the highest value among all curves and shows two peaks that correspond to through-plane blood flow during systole and diastole. Comparing the two SMS 2 curves; during systole, the blood flows through the apex slice first and then the mid slice, therefore, the mid-slice SI is lower in SMS 2 acquiring mid and apex slices than SMS 2 acquiring mid and basal slices. During diastole, the blood flows from the basal slice to the mid slice, so the blood SI appears lower in SMS 2 acquiring mid and basal slices than SMS 2 acquiring mid and apex slices. SI curve of SMS 3 has

the overall lowest value among all curves largely because of inflow blood being saturated during both systole and diastole.

**VIDEO S1.** Cine videos reconstructed with different regularization parameters. An SMS 3 dataset acquired with  $FA = 120^\circ$  reconstructed with different parameters is shown. The reconstruction parameters used for each video are presented on the top of each video. The video with selected reconstruction parameters is marked by a white box. The videos reconstructed with low  $\lambda_s$  have a high noise level and the videos reconstructed with high  $\lambda_s$  are over smoothed. The videos reconstructed with a low  $\lambda_t$  have remaining artifact while the videos reconstructed with a high  $\lambda_t$  are temporally oversmoothed. The selected parameters balanced the noise level and the temporal blurring.

**VIDEO S2.** Representative comparison of mid short-axis cine movies acquired with single band, SMS 2, and SMS 3 at flip angle of  $120^\circ$ . Images between single band and SMS 2 and 3 have no visual image quality difference and slightly different flow effects. This is because the images were acquired with different RF durations and slice encoding gradients. LV-myocardium contrast is slightly different as expected, with the SMS excitation saturating the outer volume of blood, which decrease the signal intensities because of inflowing blood.

**VIDEO S3.** Cine movies acquired from all subjects with different SMS factors at  $FA = 120^\circ$ . We have achieved consistent good quality cines from all subjects and all SMS factors. The cine from subject three with single band is blurred because of non-cooperative breath-hold. There is also relatively high flow artifact in the LV blood from subject six with SMS 2.

**VIDEO S4.** Representative comparison of mid short-axis cine movies acquired with single band, SMS 2, and SMS 3 at different flip angles. For single band image, the apparent contrast is higher with a higher flip angle. For SMS, the contrast increase with FA is present but reduced compared to single band. The overall image contrast is slightly less in SMS than single band. As FA goes up, the RF duration has to be elongated to reduce the peak  $B_1$ , which increases the flow artifacts.

**How to cite this article:** Tian Y, Cui SX, Lim Y, Lee NG, Zhao Z, Nayak KS. Contrast-optimal simultaneous multi-slice bSSFP cine cardiac imaging at 0.55 T. *Magn Reson Med*. 2023;89:746-755. doi: 10.1002/mrm.29472